The Fargo Method for Keplerian Advection: Error Analysis and Correction

Karim Shariff[1] and Alan Wray[1]

[1]*NASA Ames Research Center*
Moffett Field, CA 94035, USA

Submitted to ApJ Supp.

ABSTRACT

The Fargo method (F. Masset 2000) alleviates the time-step constraint due to Keplerian advection by shifting flow quantities an integer number of grid intervals in the azimuthal direction. We point out that the implied change of azimuthal coordinate means that all radial derivatives must carry an extra operator, $\mathcal{X} = -(t - t_0)(\partial \overline{\Omega}(r)/\partial r)\partial/\partial \phi$, which is not present in current implementations and therefore implies an error. Here t_0 is time at the beginning of a time step, $\overline{\Omega}(r)$ is the rotation rate in the coordinate transformation, and ϕ is the azimuthal coordinate. If the quantity $\partial \overline{\Omega}(r)/\partial r$ were smooth, the factor $(t - t_0)$ would imply that the error is first-order in time. However, integerization in the original Fargo scheme means that $\partial \overline{\Omega}(r)/\partial r$ is a δ-function wherever $\overline{\Omega}(r)$ suffers a jump, and so the error becomes unbounded (but more localized) in a finite-difference or finite-volume setting as the radial grid-size $\Delta r \to 0$. Numerical tests showed that the original Fargo method produces noticeable errors where $\overline{\Omega}(r)$ has a jump. These errors are advected by the flow into the rest of the domain. Even if integerization were not employed, the Fargo code is second-order in time and evaluates transport terms at $t - t_0 = \Delta t/2$; therefore the extra operator $\mathcal{X}$ still cannot be neglected. The correction proposed here is to perform a continuous-in-r shift at the end of each time step using an FFT and to include the additional operator. Simulation tests including cpu times are provided for a scheme which is fourth-order in space and time.

Keywords: Protoplanetary disks

1. MOTIVATION

The Keplerian rotation speed in cold disks can be tens of times the sound speed, which in turn can be many times the amplitude of hydrodynamic or magnetohydrodynamic turbulence. This imposes a severe limitation on the simulation time step. To alleviate this, F. Masset (2000) proposed an effective, efficient, and easy to implement technique called Fargo (Fast advection in rotating gaseous objects) which is the basis of an extensively used code of the same name. The Fargo method is also one among many options available in the hydrodynamic module of the Pluto code (Mignone et al. 2007, p. 232).

Consider the evolution equation in cylindrical coordinates of a typical quantity, the radial momentum per unit volume,

$$\frac{\partial}{\partial t}(\rho u_r) + \frac{1}{r}\frac{\partial}{\partial \phi}(\rho u_\phi u_r) + \frac{1}{r}\frac{\partial}{\partial r}(r\rho u_r^2) - \frac{\rho u_\phi^2}{r} = -\frac{\partial p}{\partial r} - \rho \frac{\partial \Phi}{\partial r}, \tag{1}$$

where Φ is the gravitational potential and other quantities have their usual meaning. Vertical derivatives have been left out for simplicity. Also, we are considering the inviscid, non-magnetic, and non-radiative situation assuming that these effects do not dominate the selection of time step. Although we are using the conservation law form, similar considerations apply to the non-conservation form. When all ϕ derivatives in the system of equations are considered

Corresponding author: Karim Shariff
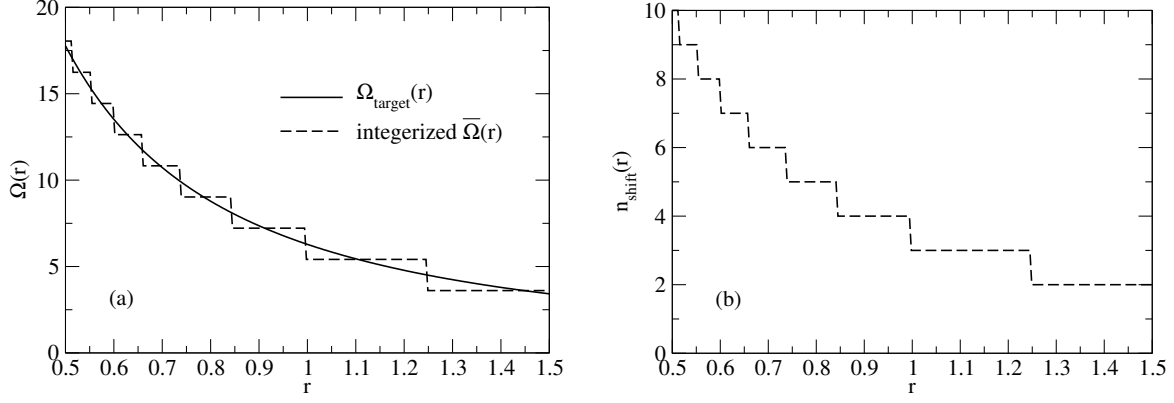karim.shariff@nasa.gov, alan.a.wray@nasa.gov

Figure 1. Properties of the original Fargo method (with integer shift) when applied to the simulation case. (a) The target and actual rotation rates. (b) Number of azimuthal shift intervals for one time step.

together, they impose the condition

$$Co_\phi \equiv \frac{C_1 \left(|u_\phi| + c_s\right)_{\max} \Delta t}{(r\Delta\phi)} < C_2, \tag{2}$$

on the time step Δt in order that numerical stability be maintained. Here Co_ϕ is the Courant number associated with the ϕ direction; C_1 and C_2 are constants that depend on the spatial differentiation and time-integration schemes, respectively. The value $C_1 = \pi$ for Fourier differentiation provides an upper limit for many classes of schemes and we henceforth assume this value. For fourth-order[1] Runge-Kutta time-integration, $C_2 = \sqrt{8}$. The term $|u_\phi|$ in (2) is dominated by the Keplerian velocity, and the goal of the Fargo method is to remove its contribution from limiting the time step. Rather than repeat the logic of the method as originally presented (F. Masset 2000), we present a discussion in terms of a coordinate transformation. This not only allows errors to be understood but also makes clear how the method can be correctly implemented.

2. ANALYSIS

Let t_0 denote time at the beginning of a step. Then, *just for the duration of the step*, a transformation of azimuthal coordinate is made

$$\phi' = \phi - \overline{\Omega}(r)(t - t_0), \quad r' = r, \quad t' = t, \quad t_0 \le t \le t_0 + \Delta t. \tag{3}$$

Choices for $\overline{\Omega}(r)$ will be described below. The only difference in the above transformation compared to that used in analytical work (Goldreich & Lynden-Bell 1965, eq. 9) is that it lasts for only one time step. At the end of the time step, one returns to the original coordinates by shifting the flow variables an amount $\phi_{\text{shift}} = \overline{\Omega}(r)\Delta t$ in the azimuthal direction.

In the original Fargo method, it is desired that the shift be an integer number of azimuthal grid intervals since such a shift is computationally efficient and easy to implement. Let $\Omega_{\text{target}}(r)$ be the target rotation velocity that one wishes to subtract out from determining the time step, and let $\Delta\phi$ be the azimuthal grid spacing. Then the closest number of grid intervals for the shift is

$$n_{\text{shift}}(r) = \text{INT}(\Omega_{\text{target}}(r)\Delta t/\Delta\phi + 0.5), \tag{4}$$

where INT is the decimal truncation function and $\Omega_{\text{target}}(r) \ge 0$ has been assumed. This corresponds to an $\overline{\Omega}(r)$ of

$$\overline{\Omega}(r) = n_{\text{shift}}(r)\Delta\phi/\Delta t, \tag{5}$$

which we refer to as being "integerized." Figure 1 illustrates $\Omega_{\text{target}}(r)$, the integerized $\overline{\Omega}(r)$, and $n_{\text{shift}}(r)$ that result for the single-vortex simulation case of §3.

---

[1] We are using a common nomenclature in which the order m of a scheme means that it is accurate to $\mathcal{O}\left(\Delta t^m\right)$ for time-integration, while for a spatial differencing it means that the truncation error is $\mathcal{O}\left(\Delta x^m\right)$.
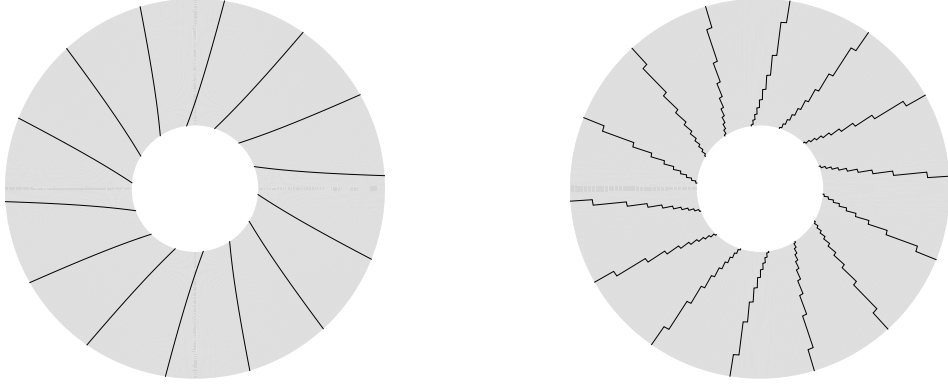
Figure 2. Lines of $\phi' = $ constant for $t > t_0$ during a time step.. Any "radial" derivatives computed in the middle of a time step should be understood to be along these lines. To make this figure we used $\Omega_{\text{target}}(r) = 2\pi(r/r_0)^{-3/2}$ (where r_0 is the mid-radius of the shaded annulus) and $(t - t_0) = 0.02$. (*Left*): Non-integerized case, i.e., $\overline{\Omega}(r) = \Omega_{\text{target}}(r)$. (*Right*): Integerized according to equation (5) with $\Delta t = 0.02$ and assuming 192 grid-points in the azimuthal direction.

The key point is that, as a result of the chain rule, derivative operators in the governing equations transform as (Goldreich & Lynden-Bell 1965, eq. 10):

$$\frac{\partial}{\partial t} = \frac{\partial}{\partial t'} - \frac{\partial \phi'}{\partial t}\frac{\partial}{\partial \phi'} = \frac{\partial}{\partial t'} - \overline{\Omega}(r)\frac{\partial}{\partial \phi'}, \tag{6}$$

$$\frac{\partial}{\partial r} = \frac{\partial}{\partial r'} - \frac{\partial \phi'}{\partial r}\frac{\partial}{\partial \phi'} = \frac{\partial}{\partial r'} - \frac{\partial \overline{\Omega}}{\partial r}(t - t_0)\frac{\partial}{\partial \phi'}, \tag{7}$$

$$\frac{\partial}{\partial \phi} = \frac{\partial}{\partial \phi'}. \tag{8}$$

It is worth keeping in mind that $\partial/\partial t$ means fixed ϕ and r, while $\partial/\partial t'$ means fixed ϕ' and r. Similarly $\partial/\partial r$ means fixed ϕ and t, while $\partial/\partial r'$ means fixed ϕ' and t. During the time step interval, flow quantities are actually located at ϕ' grid locations. Therefore any radial derivatives computed by the code in the middle of the time step are in fact $\partial/\partial r'$, and these derivatives are not along straight radial lines but along distorted ones; see Figure 2. This provides an intuitive picture useful for guiding correct implementation.

Substituting (6)–(8) into (1) gives

$$\frac{\partial}{\partial t'}\left(\rho u_r\right) + \frac{1}{r}\frac{\partial}{\partial \phi}\left(\rho u_\phi' u_r\right) + \frac{1}{r}\frac{\partial}{\partial r}\left(r\rho u_r^2\right) - \frac{\rho u_\phi^2}{r} = -\frac{\partial p}{\partial r} - \rho\frac{\partial \Phi}{\partial r}, \tag{9}$$

where

$$\frac{\partial}{\partial r} = \frac{\partial}{\partial r'} - \frac{\partial \overline{\Omega}}{\partial r}(t - t_0)\frac{\partial}{\partial \phi} \equiv \frac{\partial}{\partial r'} + \mathcal{X}. \tag{10}$$

The presence of the residual velocity,

$$u_\phi' \equiv u_\phi - \overline{\Omega}(r)r, \tag{11}$$

in the second term of (9) means that the goal of reducing the advective velocity has been achieved. However, every radial derivative contains an extra operator, denoted by $\mathcal{X}$ in (10) for subsequent brevity.

The extra operator $\mathcal{X}$ is not present in the original (integerized) Fargo formulation. What is the error due to its omission? Consider a transport term and the effect of an integerized $\mathcal{X}$ on the variable q:

$$\frac{\partial q}{\partial t} = (t - t_0)\frac{\partial \overline{\Omega}}{\partial r}\frac{1}{r}\frac{\partial}{\partial \phi}\left(rqu_r\right). \tag{12}$$

Consider a finite-volume scheme in r and let $[r_0, r_1]$ be a grid cell in r with $\Delta r \equiv (r_1 - r_0)$. Let a jump in $\overline{\Omega}(r)$ occur in the middle of the cell at $r_{1/2} \equiv (r_0 + r_1)/2$. Hence $\partial \overline{\Omega}(r)/\partial r = (\overline{\Omega}_1 - \overline{\Omega}_0)\delta(r - r_{1/2})$, where δ is the Dirac delta. Integrating (12) in r over the cell gives

$$\frac{\partial \overline{q}}{\partial t} = (t - t_0)\frac{(\overline{\Omega}_1 - \overline{\Omega}_0)}{\Delta r}\left[\frac{\partial}{\partial \phi}(qu_r)\right]_{r_{1/2}}, \tag{13}$$

where

$$\overline{q} \equiv \frac{1}{r_{1/2}\Delta r}\int_{r_0}^{r_1} q\,r dr, \tag{14}$$

is the cell average of q. Fargo is a finite-volume code and requires evaluation of the right-hand-side of (13) at $t + \Delta t/2$ (Benítez-Llambay & Masset 2016, their eq. 39). The difficulty, however, is that the right-hand-side of (13) is unbounded as $\Delta r \to 0$.

The error can be reduced if one performs a shift that is continuous in r. In this case the coefficient $C(r) = -(t - t_0)\partial\overline{\Omega}/\partial r$ is $\mathcal{O}(\Delta t)$, and so the contribution of the $\mathcal{X}$ operator to the advanced field is $\mathcal{O}(\Delta t^2)$. Most codes use time-integration schemes that are second-order or higher. Therefore it is not enough to simply use a continuous shift; one should also include the extra operator $\mathcal{X}$. Therefore, to completely eliminate the error we propose:

Corrected Scheme. (i) Make $\overline{\Omega}(r)$ exactly equal to $\Omega_{\text{target}}(r)$ so that the shift $\phi_{\text{shift}} = \overline{\Omega}(r)\Delta t$ is real-valued and continuous in r. This shift, which is needed only at the end of each time-step, can be efficiently implemented using an FFT (fast Fourier transform). (ii) Include the extra operator $\mathcal{X}$ which involves taking ϕ derivatives of flow quantities; this is possible since the coefficient $\partial\overline{\Omega}/\partial r$ is now a smooth function.

Remarks.

1. From Figure 1 one can infer that if the radial size of the computational domain is sufficiently narrow, both n_{shift} and the integerized $\overline{\Omega}$ are constant in r and t, i.e., do not undergo a jump. In this case, the original Fargo implementation is error-free, highly efficient, and should be used.

2. The original Fargo implementation used the azimuthally averaged angular velocity during the simulation for Ω_{target}, which would make it a function of both r and t in general. This means that even more terms come into play in the chain-rule differentiation which were left out in the original Fargo implementation. Here, for simplicity, we have taken $\Omega_{\text{target}}(r)$ to be time-independent.

3. Suppose one uses $e \equiv e_{\text{int}} + \rho\mathbf{u}^2/2$ for the energy variable, where e_{int} is the internal energy per unit volume. The evolution equation for e is

$$\frac{\partial e}{\partial t} + \frac{1}{r}\frac{\partial}{\partial \phi}\left[(e + p)u_\phi\right] + \frac{1}{r}\frac{\partial}{\partial r}\left[r(e + p)u_r\right] = -\rho\nabla\Phi \cdot \mathbf{u}. \tag{15}$$

The change to primed coordinates then gives

$$\frac{\partial e}{\partial t'} + \frac{1}{r}\frac{\partial}{\partial \phi}\left[(e + p)u_\phi'\right] + \overline{\Omega}(r)\frac{\partial p}{\partial \phi} + \frac{1}{r}\frac{\partial}{\partial r}\left[r(e + p)u_r\right] = -\rho\nabla\Phi \cdot \mathbf{u}, \tag{16}$$

where (10) is implied. The difficulty lies with the third term in (16). We have for an ideal gas

$$\frac{\partial p}{\partial \phi} = \frac{\partial e}{\partial \phi}\left(\frac{\partial p}{\partial e}\right)_\rho = (\gamma - 1)\frac{\partial e}{\partial \phi}. \tag{17}$$

Hence the third term in (16) implies advection at a substantial fraction of the Keplerian speed. To avoid this issue, e_{int} can be used for the energy variable instead.

4. *Self-gravity.* Regarding the gravity term in (1), if $g_r = -\partial\Phi/\partial r$ is explicitly known (for example as $-GM/r^2$), then, of course, the chain rule does not affect it. However, if a Poisson equation needs to be solved in the middle or end of a step (required for a high-order integrator), it must be remembered that the density ρ on the right-hand-side of the Poisson equation sits at ϕ' grid locations.
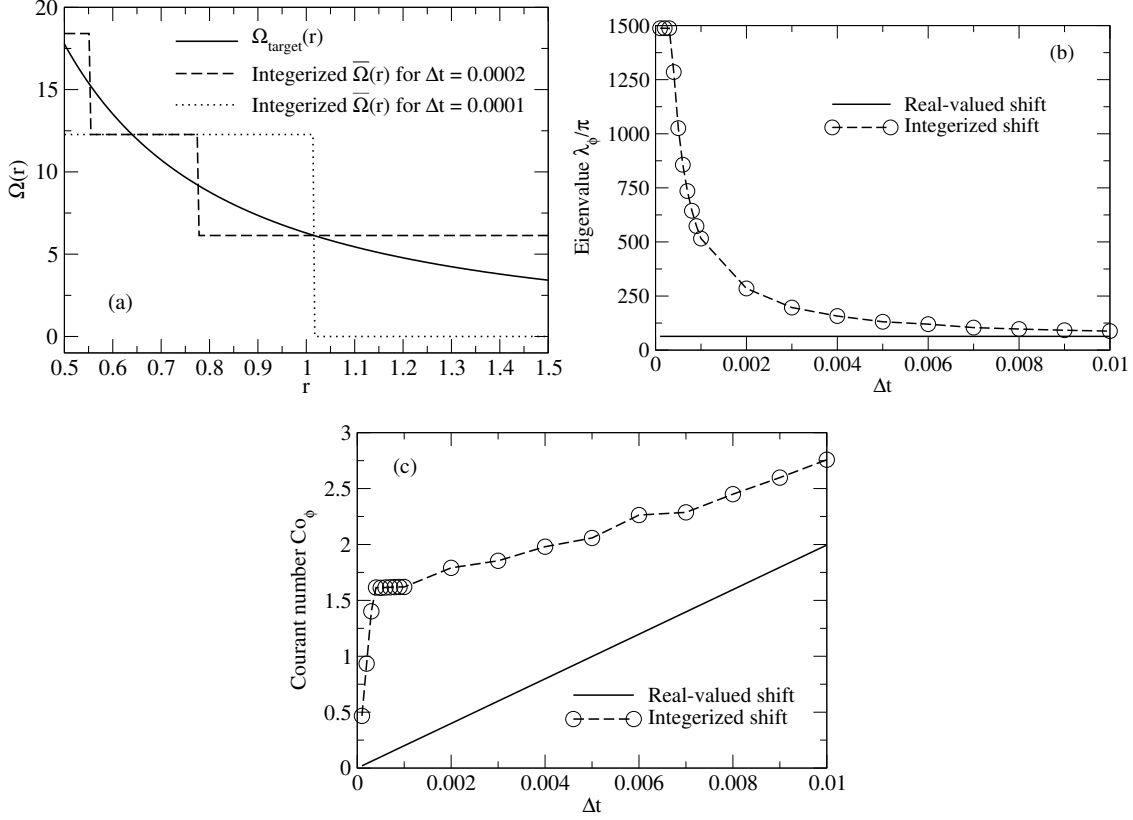
Figure 3. (a) Integerized rotation rate when the time step is reduced from 0.0002 to 0.0001, showing the increase in the difference relative to the target. (b) Response of the eigenvalue λ_ϕ and (c) Courant number Co_ϕ to reducing time step. Note that the Courant number of the integerized scheme remains high even for a small $\Delta t = 0.001$.

5. To obtain the Courant constraint associated with the extra operator acting on advective terms note that this operator acts on radial fluxes. Hence

$$Co_\chi = \pi \Delta t^2 \left| \frac{\partial \overline{\Omega}(r)}{\partial r} \right| \left(|u_r| + c_s \right) / \Delta \phi < C_2, \tag{18}$$

which can be included in the code along with the other Courant constraints. It was found to be very weak for the simulation cases shown below.

6. *A flexibility issue in the original Fargo scheme.* In the integerized-shift approach of the original Fargo scheme, the residual $|\Omega_{\text{target}}(r) - \overline{\Omega}(r)|_{\max}$ increases when the time step is reduced. It remains zero by definition for the real-valued shift proposed here. This is shown in Figure 3a for the single-vortex simulation case: when Δt is reduced from 0.0002 to 0.0001, the residual doubles (solid minus dotted lines). The result of this is that for the integerized scheme, the maximum eigenvalue λ_ϕ of the spatially discretized azimuthal flux terms increases as the the time step is reduced; see the dashed line in Figure 3b. On the other hand, the eigenvalue remains constant for a real-valued shift (solid line). The eigenvalue is defined such that the Courant number $Co_\phi = \lambda_\phi \Delta t$ and can be read-off from the time step constraint equation (2). At the left end of Figure 3b, λ_ϕ becomes a very large constant when $n_{\text{shift}}(r)$ becomes zero. Figure 3c shows the corresponding Courant number. For a given time step Δt, the real-valued shift gives a smaller Courant number. In particular, for a real-valued shift (solid line) one has the freedom to reduce the time step to satisfy the Courant condition required by the numerical method. For example, suppose that the numerical method requires $Co_\phi < 1$. For a real-valued shift one would choose $\Delta t < 0.005$, however, for an integer shift one would need a much smaller $\Delta t < 0.0002$ and indeed at this point the integer shift n_{shift} has become zero.

Run type	Δt	Co_ϕ	No. steps	cpu secs./step
Baseline. No Fargo.	3.4×10^{-4}	1.59	1000	0.121
Original Fargo (integer shift, no extra operator).	6.8×10^{-3}	2.41	50	0.128
Real shift. No extra operator.	6.8×10^{-3}	1.36	50	0.135
Corrected Fargo (real shift + extra operator).	6.8×10^{-3}	1.36	50	0.163

Table 1. Single-vortex simulation cases. In all cases the time step Δt was specified and Co_ϕ is the resulting azimuthal Courant number maximized over the mesh; this dominated the time-step selection for all simulations. The definition of Co_ϕ uses u_ϕ for the baseline run and u'_ϕ for the three Fargo runs. Cpu time is for a single core on a 2.8 GHz Intel Core i7 processor. The time excludes file input/output.

3. SIMULATION TESTS

Inviscid simulations of the vertically integrated disk model were performed. The symbol ρ denotes the vertically integrated density. There are two types of simulations. In the first, the initial condition consists of a single vortex superimposed on a nearly-Keplerian basic state. In the second, requested by the referee and inspired by the set-up of Seligman & Laughlin (2017), there are two co-rotating vortices. The numerical method is described in Appendix §A. The flow will be depicted by plotting the vortensity, ω_z/ρ, where

$$\omega_z \widehat{\mathbf{z}} = \nabla \times \mathbf{u}, \tag{19}$$

is the vorticity. In the vertically integrated disk model, as for the two-dimensional Euler equations, the vortensity obeys the equation

$$\frac{D}{Dt}\left(\frac{\omega_z}{\rho}\right) = \frac{\nabla\rho \times \nabla p}{\rho^3}, \tag{20}$$

where $D/Dt \equiv \partial/\partial t + \mathbf{u}\cdot\nabla$ denotes the derivative following fluid elements and p is the pressure. The right-hand-side of equation (20) represents baroclinic torque.

3.1. *Set-up for a single vortex*

The domain of the flow is the annulus $r \in [r_{\min}, r_{\max}] = [0.5r_0, 1.5r_0]$, where r_0 is the mid-radius of the annulus. The number of grid points $n_r \times n_\phi = 256 \times 512$. The condition of zero normal velocity was imposed at the inner and outer radial boundaries. Corresponding to the units of mass, length, and time we can set three quantities to unity. For this we chose $r_0 = T_0 = \rho_0 = 1$, which are the mid-radius, the orbital period, and density at mid-radius, respectively. The initial condition consists of a basic state and superimposed vortex. The following density and isothermal sound speed were assumed for the basic state:

$$\rho(r) = \rho_0 \left(\frac{r}{r_0}\right)^{-3/2}, \qquad c_i(r) = c_{i0}\left(\frac{r}{r_0}\right)^{-1/4}. \tag{21}$$

The value of c_{i0} is obtained by specifying the Mach number of the Keplerian flow to be

$$M_0 \equiv \Omega_K(r_0)r_0/c_{i0} = 30. \tag{22}$$

The velocity of the basic state is the nearly-Keplerian flow defined by

$$u_\phi^2(r) = u_K^2(r) + \frac{r}{\rho}\frac{\delta p}{\delta r}, \qquad u_K(r) \equiv (GM/r)^{1/2}, \tag{23}$$

in order to satisfy radial balance. Here $\delta/\delta r$ denotes a numerical derivative.

Superimposed on the basic state is a vortex centered at r_0 and $\phi = 0$; see Figure 4. Let (s, θ) denote polar coordinates centered on the vortex. The circumferential velocity $u_\theta(s)$ of the vortex is chosen to be an Oseen vortex (Batchelor 1967, p. 204) with a cut-off:

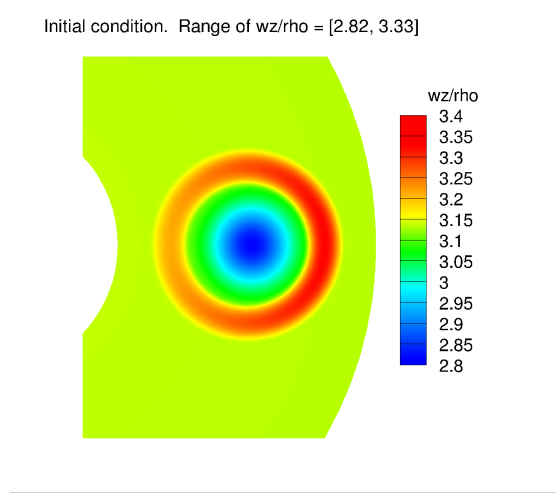$$u_\theta(s) = \frac{\Gamma}{2\pi s}\left[1 - \exp(-s^2/\sigma^2)\right] F_c(s). \tag{24}$$

Initial condition. Range of wz/rho = [2.82, 3.33]

Figure 4. Vortensity ω_z/ρ in the initial condition.

Here

$$F_c(s) = \begin{cases} 1, & s < s_c \\ g_\kappa \left[(s - s_c)/(s_{\max} - s_c)\right], & s_c \leq s < s_{\max} \\ 0, & s \geq s_{\max} \end{cases} \tag{25}$$

is a cut-off function that ensures a zero vortex velocity beyond $s = s_{\max}$. This is necessary to ensure that the vortex does not violate the condition of zero normal velocity imposed at the boundaries of the computational domain. As a result, the net circulation and (by Stokes' theorem) the net vorticity of the vortex is zero. In other words, there is a sheath of opposite sign vorticity for $s_c \leq s < s_{\max}$. For the drop-off function, g_κ, we used

$$g_\kappa(\eta) = 1 - \exp\left[-\kappa\eta^{-1}\exp\left(1/(\eta - 1)\right)\right], \qquad \kappa = (\exp 2)(\ln 2)/2, \qquad 0 \leq \eta \leq 1, \tag{26}$$

recommended by Melander et al. (1987) because it smoothly drops from 1 to 0 and all of its derivatives vanish at $\eta = 0$ and $\eta = 1$. This makes $u_\theta(s)$ a C^∞ smooth function. We chose $s_{\max} = 0.8(r_{\max} - r_0)$; in other words, the vortex ends at 0.8 times the distance from the vortex center to the domain boundaries. We also chose $s_c = 0.5s_{\max}$ so that the g_κ drop occurs over the outer half of the vortex. The width of the Gaussian is chosen to be $\sigma = 0.25s_{\max}$. To set the strength Γ of the vortex we chose the peak vorticity in the vortex $\omega_{\max} = \Gamma/(\pi\sigma^2) = -0.10\omega_0$, where $\omega_0 = (GM/r_0^3)^{1/2}/2 = \Omega_K(r_0)/2$ is the Keplerian vorticity at mid-radius which equals π for our choice of parameters. Note that the vortex is weak relative to the Keplerian vorticity and the negative sign makes it anti-cyclonic, i.e., the sense of fluid rotation it induces is clockwise while the Keplerian flow is counter-clockwise.

3.2. *Results for a single vortex*

Table 1 lists the four cases, all of which were run up to $t = 0.34$, the Keplerian orbital time at mid-radius being unity. The baseline case does not use Fargo and requires a small time step of $\Delta t = 3.4 \times 10^{-4}$ to satisfy the Courant condition. The three other cases use different types of Fargo with a 20 times larger time step. This ratio was chosen by allowing the code (run for a real valued shift) to choose its own time step based on a specified Courant number. It reported that the shift would allow a 23 times larger step which we rounded down to 20. We then ran the four cases with a fixed Δt.

Figure 5 shows the computed solution for the four cases. The original Fargo method (pane b) produces anomalous streaks at radii where $n_{\text{shift}}(r)$ undergoes a jump; the streaks are highlighted by the rectangles. For plots (a), (c), and (d) the range of ω_z/ρ changes in the third digit. This is consistent with the small value of the baroclinic term whose maximum range was found to be $\approx [-0.01, 0.01]$. The original Fargo method produces a slightly greater change in the range of ω_z/ρ.

To bring out finer features, Figure 6 plots the pointwise difference relative to the baseline. Since it is the fluctuation relative to Keplerian flow that is important in disks, we now compare the maximum difference (in absolute value) to
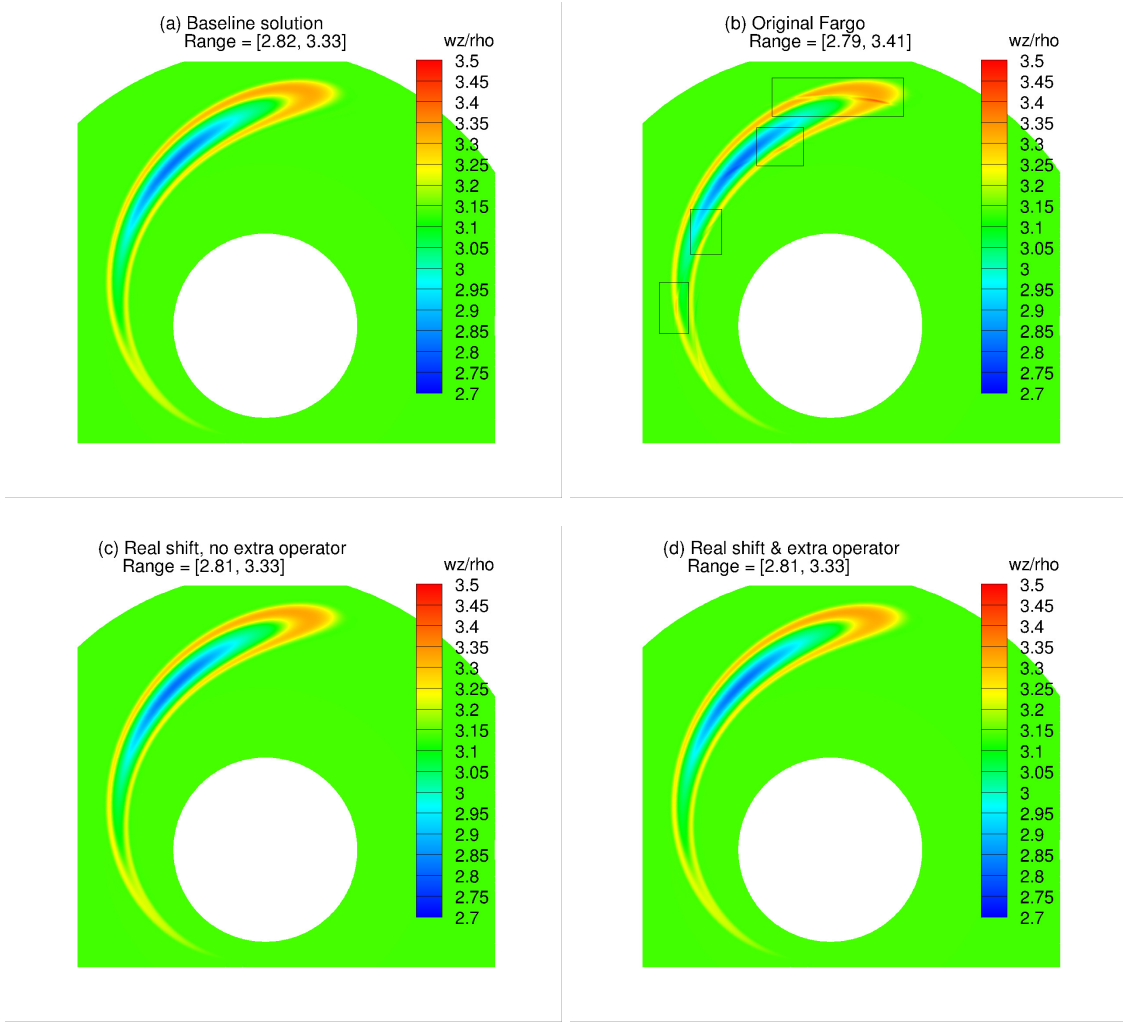
Figure 5. Single vortex case. The plots show the vortensity ω_z/ρ at $t = 0.34$ calculated using various methods. The boxes in pane (b) highlight the anomalous streaks produced by jumps in $n_{\text{shift}}(r)$ in the original Fargo method.

the maximum value of $|\omega_z/\rho - \omega_0/\rho_0|_{\max} \approx |2.82 - \pi| = 0.32$ in the initial flow, i.e., subtracting the large Keplerian contribution to ω_z/ρ. Figure 6a shows that the anomalous streaks produced by the integer shift method have a relative maximum difference (rmd) of $0.097/0.32 = 30\%$ localized most prominently at the four outermost radii where jumps in $\overline{\Omega}(r)$ occur ($r \approx 0.75, 0.85, 1.0$, and 1.25). Real-valued shifting (Figure 6b) by itself (without the extra operator) reduces the rmd to $0.0083/0.32 = 2.6\%$ and is 8% more computationally expensive than the integer shift. Finally, for the corrected Fargo method (real-valued shift with extra operator), the rmd is $0.0041/0.32 = 1.3\%$. The difference is in the form of unphysical Gibbs oscillations at the Nyquist wavelength (twice the grid spacing). This arises due to filter mismatch. Specifically, the overall effect of the small-scale filter (described in Appendix §A) applied at every step is not the same in the baseline run (with 1000 steps) and the Fargo runs (with 50 steps). It is, in fact, the baseline run that has the wiggles. The corrected Fargo method is 27% more expensive than the original Fargo method.

3.3. Co-rotating vortex pair

The referee requested that we also simulate a pair of co-rotating vortices using the set-up of Seligman & Laughlin (2017, hereafter SL). The profile used by SL has a jump in vorticity and produced relatively large unphysical Gibbs oscillations in our simulations; these oscillations can also be seen in Figure 8 of SL. We therefore reverted to using the Gaussian-based profile (24) of our single vortex test case. Note that the SL simulation was performed in a rotating Cartesian box with shear-periodic boundary conditions, while the present code is in cylindrical coordinates. In the
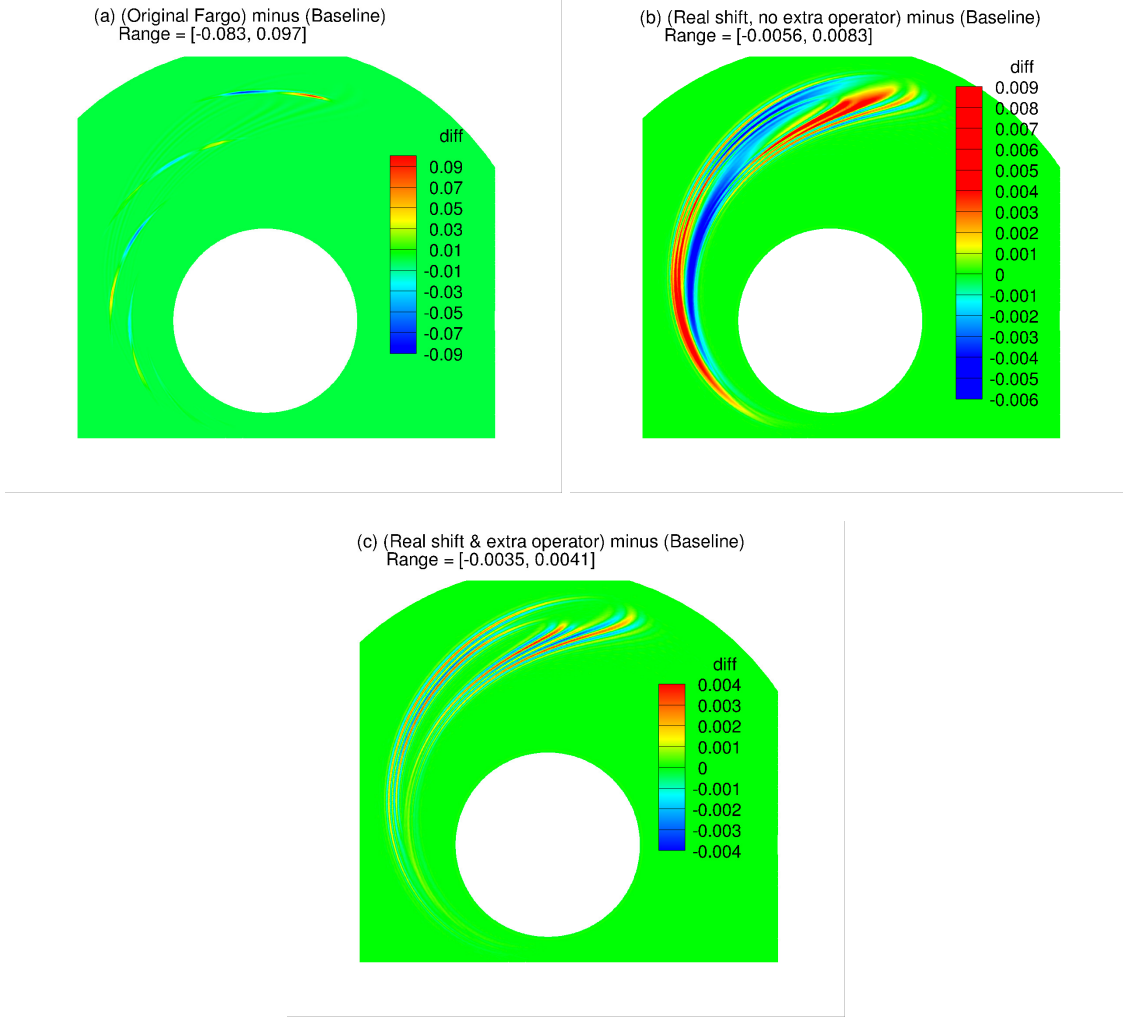
Figure 6. Differences in ω_z/ρ of various methods relative to the baseline run ($t = 0.34$).

shearing-box context, the issue of a time-step restriction due to Keplerian advection does not arise. The present computational domain is $r \in [r_{\min}, r_{\max}] = [0.96, 1.04]r_0$ (with $r_0 = 1$) $\times \phi \in [0, 2\pi/79] \approx [0, 0.08]$ radians. This is twice larger than SL to ensure that the original Fargo method produces a jump in $n_{\mathrm{shift}}(r)$ within the computational domain, otherwise a comparison of methods would be moot. The number of grid points is $n_r \times n_\phi = 512 \times 512$. Boundary conditions are periodic in the azimuthal (ϕ) direction and zero normal velocity at $r = r_{\min}$ and $r = r_{\max}$. The initial condition consists of a basic state and two vortices. The basic state has uniform density $\rho(r, \phi) = \rho_0 = 1$ and a Keplerian velocity $u_\phi = (GM/r)^{-1/2}$ with $GM = 1$. Note that these choices make the angular velocity, Ω_0, at mid-radius equal to unity. Therefore the orbital period and Keplerian vorticity at this location are $T_0 = 2\pi$ and $\omega_0 = 1/2$, respectively. The equation of state is taken to be isothermal, i.e., $p = \rho c_{i0}^2$ with a uniform $c_{i0} = 0.05$. Unlike the single-vortex test, this implies barotropic flow and therefore preservation of ω_z/ρ following the fluid.

Two vortices with centers at $(r, \phi) = (1 \pm 0.005, 0.04 \pm 0.010)$ are added to the basic state. To satisfy periodicity, their images in the azimuthal direction are also included. The strength of each vortex, $\Gamma = -0.04/30$, was chosen to obtain the same vorticity at the vortex center as SL. The negative sign means its sense of rotation is clockwise, i.e., opposite to the Keplerian flow. The width of the Gaussian $\sigma = 0.005$ and the parameters of the cut-off function $F_c(s)$ were taken to be $s_c = 0.006$ and $s_{\max} = 0.012$. Figure 7 shows that the circumferential speed and vorticity profiles contributed by each vortex are C^∞ smooth, the vorticity is negative in the center, and there is a sheath of positive vorticity at the edge of the vortex. The eddy turnover period at the location of maximum $|u_\theta|$ is $T_{\mathrm{eddy}} \approx 2\pi/(0.026/0.006) \approx 1.5$.
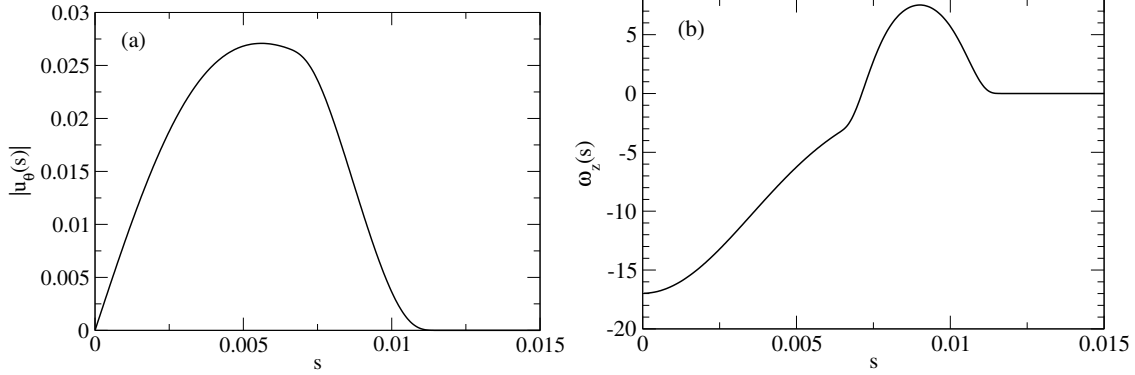
Figure 7. Set-up for the co-rotating vortex pair simulation. Profiles of (a) circumferential speed, $|u_\theta(s)|$, and (b) resulting vorticity, $\omega_z(s)$, contributed by each member of the vortex pair, s being the distance from the vortex center. Equation (24) is used for $u_\theta(s)$ with the parameter values given in the text.

Run type	Δt	Co_ϕ	No. steps to $t = 0.4$	cpu secs./step
Baseline. No Fargo.	9.75×10^{-5}	2.20	4104	0.286
Integer shift. No extra operator.	3.9×10^{-4}	2.16	1026	0.299
Real shift + extra operator.	3.9×10^{-4}	0.614	1026	0.389

Table 2. Co-rotating vortex pair simulations. For explanation of quantities, see the caption for Table 1.

Table 2 lists the runs performed for the co-rotating vortex pair. The case of a real-valued shift without the extra operator was not considered since the single vortex case has already established that the extra operator is required to obtain an accurate result. Note that for the same value time step Δt, the Courant number of the corrected scheme (real-valued shift with extra operator) is more than three times less than the original Fargo scheme. This is because with a real-valued shift, there is no difference between the target and actual $\overline{\Omega}(r)$. This means that the corrected scheme could have been run with a three times larger time-step without affecting numerical stability.

Since there is current interest in the vorticity preservation properties of various numerical schemes (Seligman & Laughlin 2017), Figure 8 provides a series of snapshots up to $t = 6$ calculated by the corrected scheme; the times chosen align roughly with the first four frames presented by SL. For later use in computing the relative error, note that the peak value of the vortensity in the initial vortices relative to the Keplerian value is $|\omega_z/\rho - \omega_0/\rho_0|_{\max} = |-16.5 - 1/2| = 17.0$. The range of vortensity should be preserved if all length scales of the flow are perfectly resolved. We see that the peak negative value in the vortex cores is very well preserved. However, the peak positive value which occurs in a thin shear layer undergoes a small increase followed by a more substantial decrease at later times. SL do not provide the range of ω_z/ρ so we cannot say how the present scheme compares with theirs. Since the maximum positive value occurs in barely resolved layers whose width is about a grid interval, we are confident that our simulations are accurate solutions of the Euler equations except in very thin unresolved layers. The applied Padé filtering (Appendix A) is a provisional sub-grid treatment that dissipates enstrophy at small scales. The testing in disk flows of various sub-grid treatments against fully-resolved viscous simulations is highly desirable, but beyond the scope of the present work.

We now compare Fargo treatments for this flow. Figure 9 shows that the integerized $\overline{\Omega}$ has only a single jump (at $r \approx 1.002$) for this case due to the smallness of the domain in the radial direction; the integerized number of shift intervals jumps from three to two. Figure 10b shows the difference in the solution of the original Fargo scheme relative to the corrected scheme. The pattern, which resembles a whirligig, suggests that the error produced by the original Fargo scheme at jumps in $n_{\text{shift}}(r)$ is advected by the flow of each vortex. The maximum relative difference is $2.11/17.0 = 12.4\%$.

Finally, we consider the error at a later time of $t = 6$ which is about four eddy turnaround times. Figures 11a and b provide a side-by-side comparison of the solutions obtained from the original and corrected schemes. The plot is zoomed-in on the right-hand vortex. In addition to the glitches produced at the jump in $n_{\text{shift}}(r)$, the right-hand
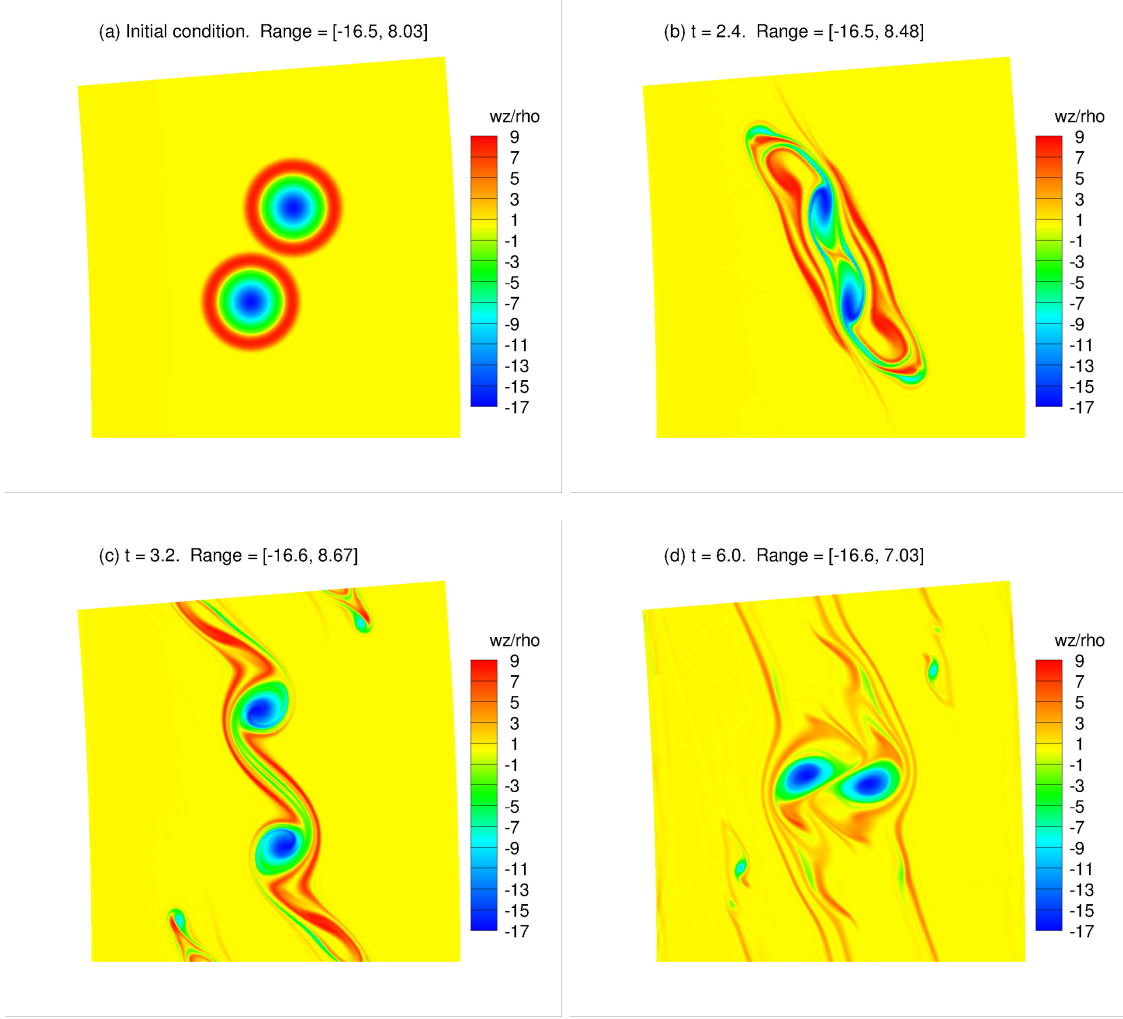
(a) Initial condition. Range = [-16.5, 8.03]

(b) t = 2.4. Range = [-16.5, 8.48]

(c) t = 3.2. Range = [-16.6, 8.67]

(d) t = 6.0. Range = [-16.6, 7.03]

Figure 8. Two co-rotating vortices simulated using the corrected Fargo scheme (real-valued shift with extra operator). Colors represent the vortensity ω_z/ρ whose range should be preserved if all scales are perfectly resolved. For plotting purposes, the azimuthal (ϕ) position of the vortensity field was shifted to remove rotation by the Keplerian angular velocity at mid-radius.
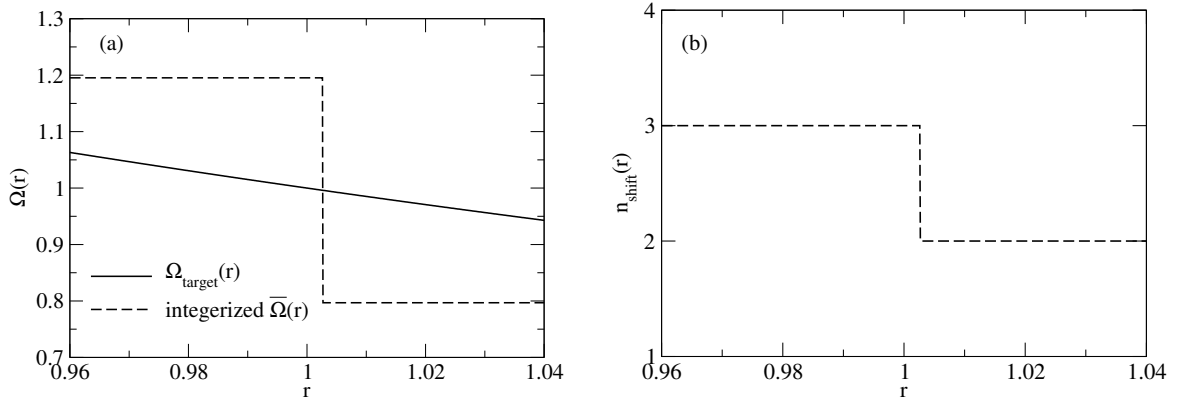
Figure 9. Properties of the original Fargo method (with integer shift) when applied to the co-rotating vortex pair case. (a) Target and integerized rotation rates. (b) Number of azimuthal shift intervals in one time step. The jump occurs at $r \approx 1.002$.
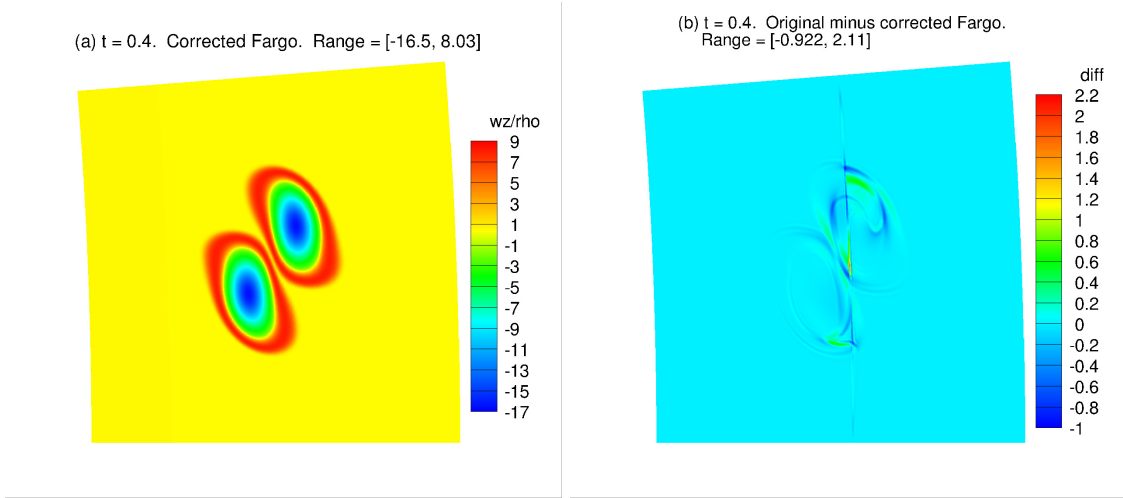
Figure 10. (a) Vortensity calculated by the corrected Fargo method at $t = 0.4$. (b) Difference in the vortensity predicted by the original Fargo scheme relative to the corrected scheme.
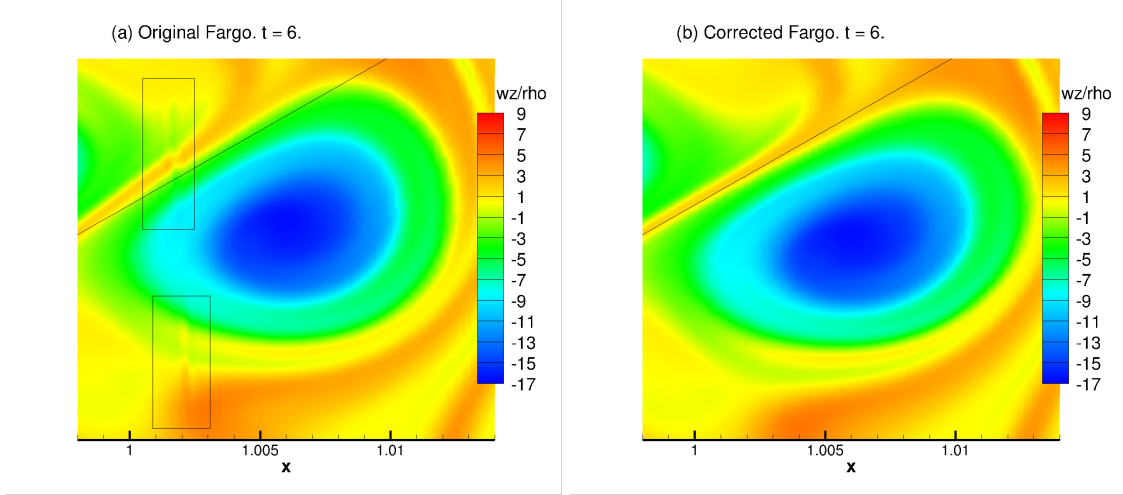

Figure 11. Comparison of solutions at $t = 6$ zoomed-in on the right-hand vortex. The black line is provided as an aid for noticing the small difference in vortex co-rotation angle. It was hand drawn in pane (b) along the lane between the two vortices and then copied into pane (a). The two boxes on the left indicate artifacts produced at the jump in $n_{\mathrm{shift}}(r)$.

vortex calculated by the original Fargo scheme lags slightly in its clockwise rotation about the other vortex. A zoom on the left-hand vortex shows that it too is lagging in its rotation about its partner. Evidently, anomalous vortensity produced at the jump in $n_{\mathrm{shift}}(r)$ has been entrained by each vortex causing a reduction in its overall strength.

4. CLOSING REMARKS

The integerized shift method (F. Masset 2000) is a clever idea for reducing the time-step restriction due to Keplerian advection. However, we have pointed out that the method implicitly assumes a change of coordinates and the chain-rule leads to an extra operator in the radial derivative, not included in current implementations. Formally, this operator cannot be ignored for second-order and higher time-integration schemes. Furthermore, integerization makes this operator unbounded (as $\Delta r \to 0$) at radial locations where the number of shift intervals undergoes a jump.

To eliminate the error, we proposed that the shift be a continuous function of r (which can be efficiently implemented using an FFT) and the additional operator be included.

Numerical tests were performed for the vertically integrated disk model using fourth-order Padé spatial differencing and fourth-order Runge-Kutta time-integration. In the single-vortex test, the original Fargo scheme (integer shift without the extra operator) produced anomalous streaks in the vortensity at radii corresponding to jumps in the integerized $\overline{\Omega}(r)$. The maximum relative error due to these streaks was 30%. Errors with 2.6% amplitude remained when a real-valued shift was performed and the extra operator was not included. With a real-valued shift and inclusion of the extra operator, the error was 1.3% compared to the baseline run which did not employ the Fargo method and used a twenty times smaller time-step. This difference was attributed to unequal filtering due to the difference in the number of time steps.

For two co-rotating vortices, the original Fargo method produced a maximum relative error of 12.4% at an early time. The errors were subsequently advected and entrained by the vortex flow, and after four eddy turnover times, in addition to glitches in the solution where $\overline{\Omega}(r)$ has a jump, there was a small error in the phase of vortex co-rotation.

The question arises as to what the errors are in codes that have implemented the original Fargo method. Numerical tests should be undertaken to study this. In codes that use a dissipative scheme, the error might be smeared and mixed into the flow but still detectable using the discrete L_2 norm ($\propto$ the sum of squares) of the difference.

REFERENCES

Batchelor, G. 1967, An Introduction to Fluid Dynamics (Cambridge, UK: Cambridge University Press)

Benítez-Llambay, P., & Masset, F. 2016, ApJS, 223, 11

F. Masset. 2000, ApJS, 141, 165

Goldreich, P., & Lynden-Bell, D. 1965, MNRAS, 130, 125

Kopal, Z. 1961, Numerical Analysis, 2nd edn. (New-York: Wiley)

Lele, S. 1992, J. Comp. Phys., 103, 16

Melander, M. V., McWilliams, J. C., & Zabusky, N. J. 1987, J. Fluid Mech., 178, 137–

Mignone, A., Bodo, G., Massaglia, S., et al. 2007, ApJS, 170, 228

Seligman, D., & Laughlin, G. 2017, ApJ, 848, 54

APPENDIX

A. NUMERICAL METHOD

The Euler equations of inviscid hydrodynamics together with the gravity of a point mass at the origin are solved in polar coordinates (r, ϕ). These equations evolve the density (ρ), angular momentum per unit volume $(\rho u_\phi r)$, and radial momentum per unit volume (ρu_r). A fixed radial temperature profile is maintained, i.e., the pressure is obtained from

$$p = \rho c_i(r)^2, \tag{A1}$$

where $c_i(r)$ is given by (21) for the single-vortex case and is constant for the vortex pair. These choices assume rapid thermal relaxation to the basic state.

Let primes denote differentiation with respect to a grid index coordinate ξ which increments by unity from one grid point to the next. This differentiation is performed using the standard fourth-order compact scheme[2] (Kopal 1961; Lele 1992):

$$\frac{1}{4} f'_{i-1} + f'_i + \frac{1}{4} f'_{i+1} = \frac{3}{2} \frac{f_{i+1} - f_{i-1}}{2} - \frac{1}{5!} \frac{\partial^5 f}{\partial \xi^5} + \dots, \tag{A2}$$

the last term being the leading-order truncation error. The derivative with respect to a physical coordinate, x say, is obtained from

$$\left(\frac{\partial f}{\partial x} \right)_i = f'_i \left(\frac{\partial x}{\partial \xi} \right)_i^{-1}, \tag{A3}$$

where the second factor is the inverse Jacobian of the grid. Compact schemes are known to have much better resolving power than usual central difference schemes of the same order. A fourth-order Runge-Kutta scheme is used for time-advancement. Since the compact scheme is non-dissipative and the inviscid equations are employed, fine scales which cannot be resolved by the mesh are generated. Their enstrophy (in two-dimensions) piles up near the Nyquist wavenumber of the mesh. To dissipate this, a compact filter (Lele 1992, p.40) with parameters $\beta = d = 0$ and α free is applied to all the field variables after each time step. To choose α we note that to leading order the filter acts a fourth-order dissipation (see the truncation error expression in Lele's table IX):

$$\widehat{f}(x) = \left[1 + \frac{1}{16} \left(1 - 2\alpha \right) h^4 \partial^4 / \partial x^4 \right] f(x), \tag{A4}$$

where is $\widehat{f}(x)$ is the filtered version of $f(x)$ and h is the grid size in the filtering direction. Next consider the following expression,

$$f(x, t + \Delta t) = \left(1 + \nu_4 \Delta t \partial^4 / \partial x^4 \right) f(x, t), \tag{A5}$$

which represents one Euler step applied to $\partial f / \partial t = \nu_4 \partial^4 f / \partial x^4$. In the spirit of sub-grid modeling, the hyperviscosity is written

$$\nu_4 = \frac{h^4}{\tau_{\text{filter}}}, \tag{A6}$$

where τ_{filter} represents the time scale at which sub-grid scales are amplified by the mean strain. Equating (A4) to (A5) we obtain

$$\alpha = \frac{1}{2} - \frac{8\Delta t}{\tau_{\text{filter}}} \tag{A7}$$

After some experimentation we chose $\tau_{\text{filter}} = 0.25$ for the single-vortex case, i.e., a quarter of the orbital period at r_0. Note the dependence of α on the time step Δt. This partially, but not completely, equalizes small-scale wiggles in the Fargo and non-Fargo (baseline) runs. This lack of complete equalization of the filter is responsible for the small-amplitude wiggles (Figure 6c) remaining when the result of the non-Fargo run (small time-step) is subtracted from the corrected-Fargo run (large time-step). For the vortex pair runs, we used $\tau_{\text{filter}} = 0.10$ due to the stronger vortices. A better sub-grid treatment should depend on local flow conditions.

---

[2] To our knowledge, this class of schemes were first considered by Zdenek Kopal, a Czech born astronomer, who obtained them using an operator calculus; see the bibliographical note on pg. 520 of Kopal (1961). Specifically, the derivative operator is expressed exactly as a function of the central finite-difference operator. This function is then written in a finite Taylor series, which is then written as a Padé approximant.